PAPER

Enhancement of Si solar cell efficiency using ZnO nanowires with various diameters

To cite this article: A Gholizadeh *et al* 2018 *Mater. Res. Express* **5** 015040

Materials Research Express

PAPER

RECEIVED
6 November 2017

REVISED
21 December 2017

ACCEPTED FOR PUBLICATION
4 January 2018

PUBLISHED
19 January 2018

Enhancement of Si solar cell efficiency using ZnO nanowires with various diameters

A Gholizadeh[1], A Reyhani[1], P Parvin[2], S Z Mortazavi[1] and M Mehrabi[2]

[1] Physics Dept., Faculty of Science, Imam Khomeini International University, PO Box 34149-16818, Qazvin, Iran
[2] Physics Dept., Amirkabir University of Technology, PO Box 15875-4413, Tehran, Iran

E-mail: reyhani@sci.ikiu.ac.ir

Keywords: ZnO nanowires, reduction of spectral reflectance, photon trapping, Si-solar cell efficiency

Abstract

Here, Zinc Oxide nanowires are synthesized using thermal chemical vapor deposition of a Zn granulate source and used to enhance a significant Si-solar cell efficiency with simple and low cost method. The nanowires are grown in various O_2 flow rates. Those affect the shape, yield, structure and the quality of ZnO nanowires according to scanning electron microscopy and x-ray diffraction analyses. This delineates that the ZnO nanostructure is dependent on the synthesis conditions. The photoluminescence spectroscopy of ZnO indicates optical emission at the Ultra-Violet and blue–green regions whose intensity varies as a function of diameter of ZnO nano-wires. The optical property of ZnO layer is measured by UV–visible and diffuse reflection spectroscopy that demonstrate high absorbance at 280–550 nm. Furthermore, the photovoltaic characterization of ZnO nanowires is investigated based on the drop casting on Si-solar cell. The ZnO nanowires with various diameters demonstrate different effects on the efficiency of Si-solar cells. We have shown that the reduction of the spectral reflectance and down-shifting process as well as the reduction of photon trapping are essential parameters on the efficiency of Si-solar cells. However, the latter is dominated here. In fact, the trapped photons during the electron–hole generation are dominant due to lessening the absorption rate in ZnO nano-wires. The results indicate that the mean diameters reduction of ZnO nanowires is also essential to improve the fill factor. The external and internal quantum efficiency analyses attest the efficiency improvement over the blue region which is related to the key parameters above.

Introduction

The zinc oxide (ZnO) is of the great interest in recent years because of the fascinating unique properties as well as its potential in practical aspects of solar cells. Bulk ZnO acts as a semiconductor that benefits a high and direct band gap (3.37 eV) with a large exciton binding energy of ~60 meV at room temperature and unique photoluminescence (PL) characteristics which crystallizes in hexagonal wurtzite structure [1]. The advantages of ZnO nanostructures in the solar cells are reported elsewhere [2–7]. ZnO nanorods have already been extensively investigated as the photo-electrodes in the organic, amorphous and dye-sensitized solar cells [8–12]. Those are efficiently utilized as the antireflective coating to suppress the spectral reflectance [13–16].

In previous work, we have investigated the function of ZnO nano-plates in down-shifting to improve efficiency of Si-solar cell [4]. One of our goals here is to investigate the effect of different structures of ZnO and to find the optimal structure for the purpose of solar cells manufacturing. Recently, zinc oxide nanostructures, including nano-plates and nano-rods, were synthesized in the presence of argon gas. Those were grown in various temperatures and Ar/O_2 flow rates. The optical properties elucidate the population of nano-plates in the samples strongly affect the band gap [4].

Table 1. ZnO nanowire synthesis conditions for samples #1–5.

Sample	Sample #1	Sample #2	Sample #3	Sample #4	Sample #5
Oxygen flow (sccm)	25	50	100	150	200

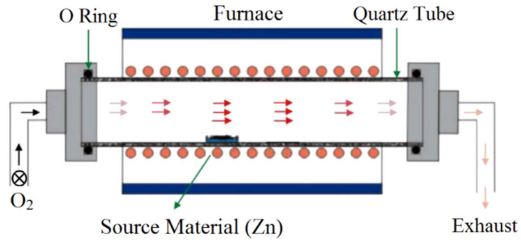

Figure 1. Schematic diagram of the electrical furnace with a horizontal tube for ZnO nanowires synthesis.

On the other hand, we intend to answer the basic questions: what is the effect of nanostructures in the absence of nano-plates and the attendance of sole nanowires? and which one is more effective structure for solar energy?

In this work the sole nanowires are synthesized in the absence of argon gas using various oxygen flow rates. The ZnO nanowires with various diameters demonstrate different optical performance (reflectance and luminescence) and thus impose different effects on the enhancement of the solar cell characteristics.

It is worth that the current manuscript deals with dominant mechanism of photon trapping and reduction of spectral reflectance while previous work has focused on the downshifting.

The ZnO nanowires are grown based on thermal chemical vapor deposition (TCVD) in different conditions to enhance the electrical properties of Si-solar cells according to the drop casting method. The enhancement of solar cell mainly arises from the reduction of the spectral reflectance and frequency shift of incident solar radiation particularly in UV (and blue) spectral regions to the longer wavelengths. It is believed that optical loss lessening accompanying the enlargement of the fill-factor (FF) due to the sensible reduction of equivalent series resistance is related to the nano-wires with lower diameters. The scanning electron microscopy (SEM), x-ray diffraction (XRD), PL and UV–vis spectrophotometry are employed to assess the structure, quality and optical properties of the ZnO nanowires. The current–voltage (I–V) characteristics as well as external and internal quantum efficiency (EQE and IQE) support the findings to diagnose of the solar cell properties for the purpose of better performance. Moreover, the diffuse reflection spectroscopy (DRS) is employed to analyze the spectral reflectance of the untreated and treated Si solar cells.

Methods

Experimental

The ZnO nanowires are fabricated using TCVD in a horizontal tube furnace. The zinc metal granulates as source material is supplied by Sigma-Aldrich, USA with a purity of 99.99%. To synthesize ZnO nanowires, the furnace temperature is ramped from the room temperature to the oxidation temperature of 900 °C, in Ar flow (200 sccm) for 20 min. After the stabilization at the oxidation temperature, the Ar flow stops and oxygen is injected into the furnace at the given temperature for 30 min. The O_2 flow rate is varies from 25, 50, 100 to 150 and 200 sccm in 30 min. Then, the furnace is allowed to cool down to the room temperature where the ZnO nanowires are taken out for the further utilization. Table 1 tabulates the synthesis conditions for the samples labeled #1–5. Figure 1 depicts the apparatus schematic for the nanostructural synthesis, including the gas inlet/outlet, sample holder, and the pathway of gas flow.

Characterization

Morphology of the nanowires is determined by SEM model philips. The XRD model Inel equinox 3000 is employed to record the crystalline structure of ZnO nanowires. PL spectrometer model Perkin Elmer LS55 and UV–vis spectrophotometer model EPP2000 is employed to inspect the optical properties of the nanowires. Also, the quantum yield (QY) of samples is measured by single point method using results of PL and UV–vis analyses. To investigate the solar cell application of the ZnO nanowires, the commercial multi-crystal silicon (1.5×6 cm^2) solar cell made by Bulisheng Company in china is coated by the nanowires using drop casting method. To provide ZnO suspension on Si-solar cell, 2.5 mg of nanowires is solved in 50 cc ethanol by means of

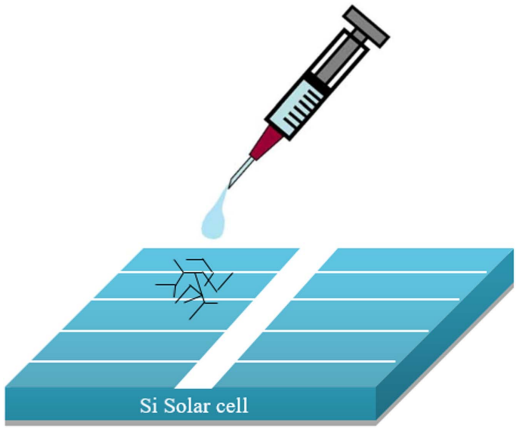

Figure 2. A schematic drop-casting of ZnO suspension.

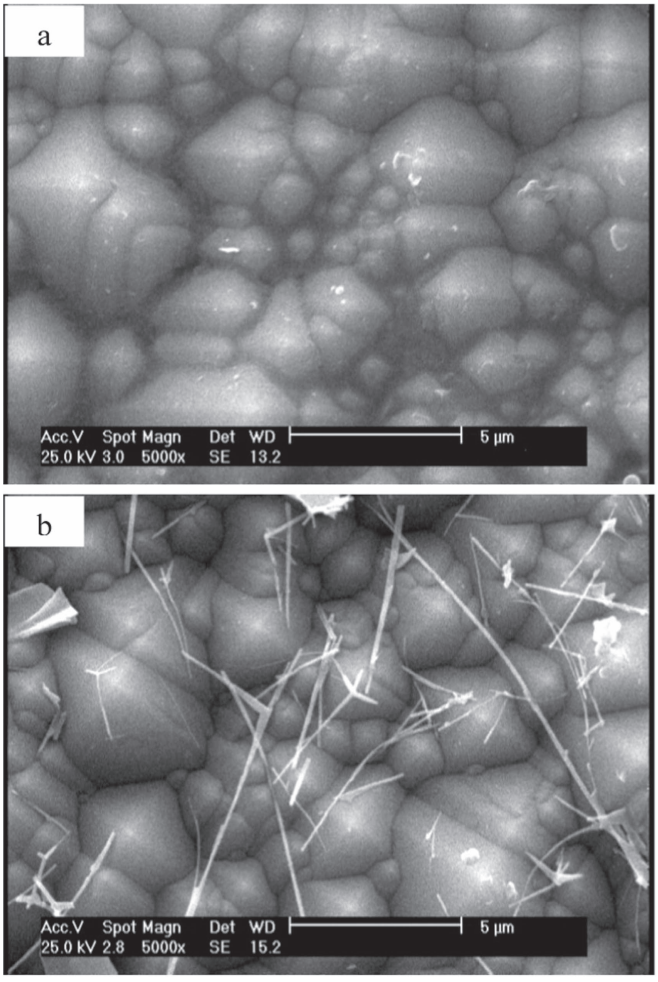

Figure 3. SEM images of Si solar cell (a) before and (b) after drop casting.

an ultrasonic homogenizer (60 W) for 5 min. Then, the ZnO is deposited on the surface with drop casting method. Figure 2 illustrates the schematic drop casting of ZnO nanostructure suspension on the Si solar cell. Figure 3 depicts SEM images of the Si solar cell before (and after) drop casting. After droplet, the I–V plot and the quantum efficiency are recoded for further analysis. The I–V characteristics of the Si solar cells are determined with (and without) ZnO nanowires using Keithley 2400 source measure unit instruments and solar simulator model Sharif Solar SIM-1000 under the standard test conditions (AM 1.5 irradiation, $T = 300$ K and $P = 1$ kW m^{-2}). The quantum efficiency is determined for several tuned lights with wavelengths of 400 $\pm$ 15,

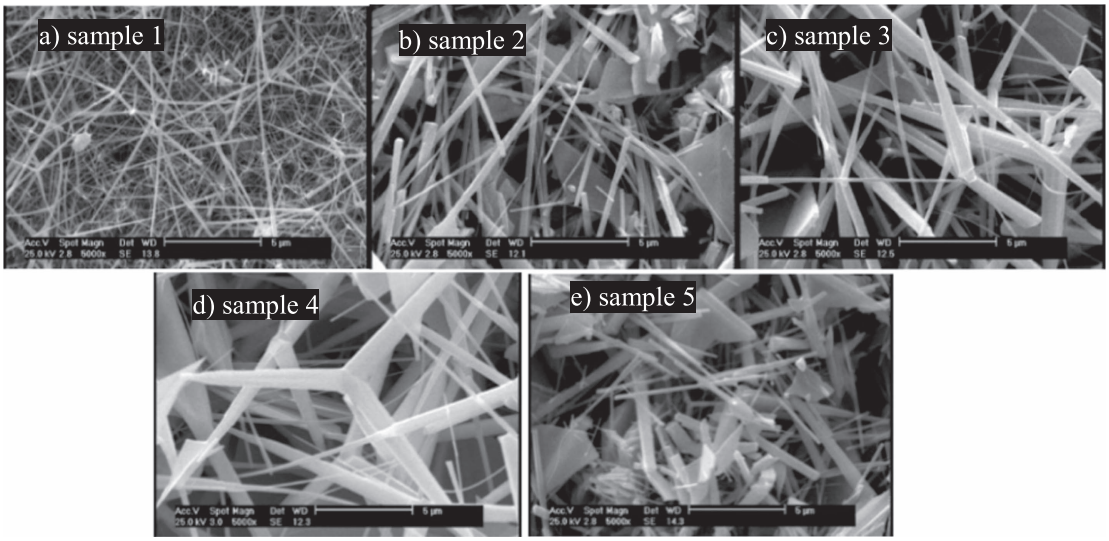

Figure 4. SEM images of ZnO nanowires prepared by TCVD at 900 °C under O_2 flow rate of (a) 25, (b)50, (c) 100, (d) 150 and (e) 200 sccm.

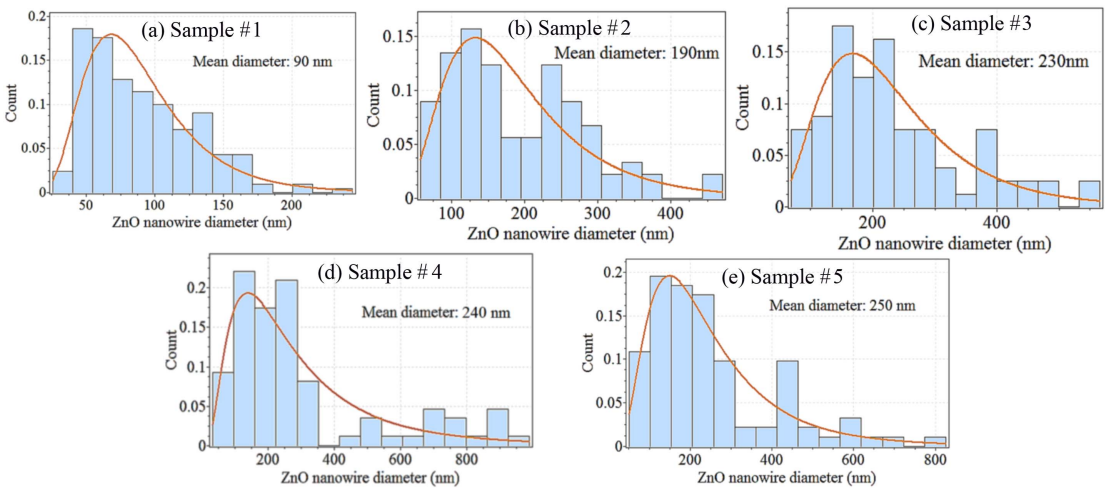

Figure 5. Histogram of size distributions of ZnO nanowire of samples #1–5.

460 ± 15, 505 ± 15, 530 ± 15 and 630 ± 15 nm using the solar simulator equipped with halogen lamp and different LED sources. The DRS model Avaspec-2048-TEC is used to study the optical reflectance of the solar cell surface.

Results and discussion

Figure 4 illustrates SEM images of the fabricated nanowires in various conditions of O_2 flow rate. Those reveal that all treated samples contain plentiful ZnO nanowires. Figure 5 depicts the size distribution of the ZnO nanowires by counting hundreds of them over different fields of the SEM images. The experimental data are fitted with the log-normal function. ZnO nanowires in samples #1, 2, 3, 4 and 5 contain a mean diameter of about 90, 190, 230, 240 and 250 nm, respectively.

Figure 6 displays the XRD pattern of the ZnO nanowires. Table 2 summarizes the diffraction peaks corresponding to the reflectance on the crystal surface. The sharp diffraction peaks at about $2\theta = 32.1°, 34.7°, 36.6°, 48.1°$ and $57.1°$ correspond to the reflectance on the crystal surfaces of (100), (002), (101), (102) and (110) respectively. Those diffraction peaks are easily assigned to a ZnO hexagonal wurtzite structure without any sensible impurity [17]. Note that the most intense peak appears at plane (100) in the samples #1 and 2 which those have got smaller diameters than the other samples. The crystallite sizes of the prepared ZnO nanowires are

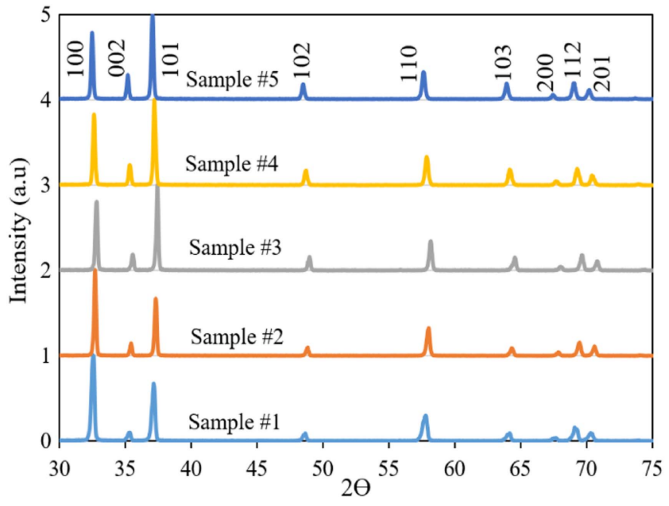

Figure 6. XRD patterns of the ZnO nanowires and the hexagonal wurtzite structure of ZnO.

Table 2. The diffraction peak position (2θ) for the crystal planes.

	100	002	101	102	110	103
Sample #1	31.9163	34.6905	36.4656	47.8697	56.9533	63.2642
Sample #2	32.0735	34.7851	36.6190	48.0618	57.1728	63.4239
Sample #3	32.1992	34.9111	36.7416	48.1898	57.3294	63.6587
Sample #4	31.9792	34.6905	36.5270	47.9337	57.0160	63.2642
Sample #5	31.8535	34.5328	36.3734	47.7096	56.7650	63.0112

Table 3. Calculated values from XRD data.

Sample	a	c	V	Strain	σ (GPa)	c/a ratio	Willamson–Hall (nm)	Preferred peak (hkl)
#1	3.233	5.172	46.815	−0.007	1.631	1.60	10.8	(100)
#2	3.219	5.154	46.249	−0.010	2.33	1.60	9.4	(100)
#3	3.209	5.136	45.802	−0.014	3.262	1.60	7	(101)
#4	3.227	5.168	46.606	−0.007	1.631	1.60	11.2	(101)
#5	3.241	5.190	47.211	−0.003	0.699	1.60	17	(101)

calculated using the full width at half maximum (FWHM) of the highest peak employing Williamson–Hall equation [18]

$$\beta \cos\theta = \frac{K\lambda}{D} + 4\varepsilon \sin\theta, \tag{1}$$

where D, λ, θ, β, K and ε are the average crystalline size, the x-ray wavelength of 1.54 Å, the Bragg diffraction angle, the FWHM, Scherrer's constant and the lattice strain, respectively. The strain (ε) along the C-axis can be given by

$$\varepsilon = \frac{(c_{\text{Powder}} - c_{\text{Bulk}})}{c_{\text{Bulk}}}, \tag{2}$$

where C_{bulk} denotes to be 5.207 A [1] for ZnO. Regarding the biaxial strain model, the stress (σ) in the ZnO powder can be determined to be $\sigma = -233\varepsilon$ [19]. Lattice parameter, crystallite size, c/a ratio and stress and strain of samples are tabulated in table 3. According to the results given by XRD and SEM, when the mean diameter of nano-wires increases, then the preferring direction is changed from (100) to (101). Tables 2 and 3 attest that the spacing between the crystallite planes lucidly varies with the nanowires diameters. Kunj *et al* reported the dependence of spacing with oxygen content [20]. In addition, table 3 indicates that the induced strain mainly relies on the shortest crystalline size. Sample #3 shows the maximum parameters, including largest strain and smallest spacing with respect to other samples. According to the tables 2 and 3, there are different grain size and strain for the samples with various diameters. Similar to previous work [4], we will show that samples, with the most intense peak, appear at plane (100). Those demonstrate the highest impact in

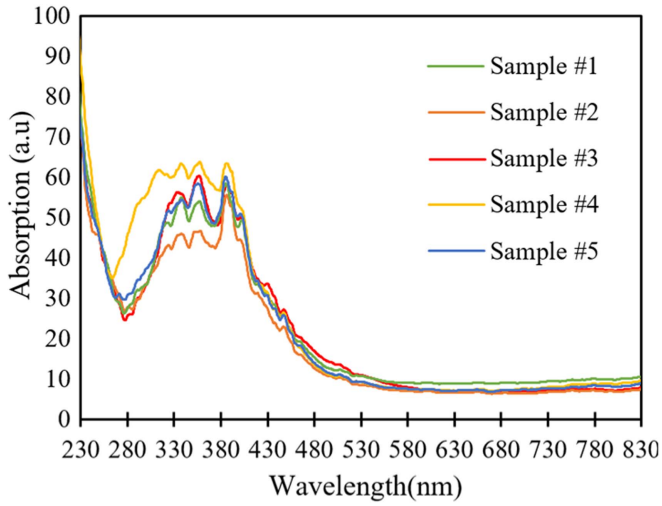

Figure 7. The optical absorption of synthesized nanowires characterized by UV–visible spectrophotometer of sample #1–5.

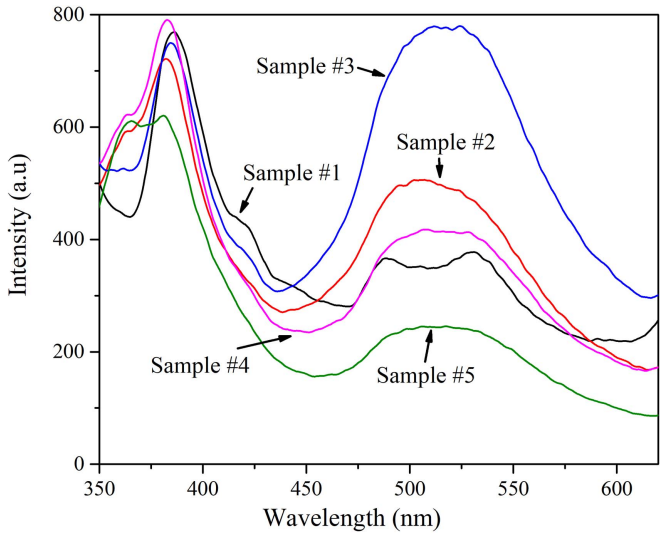

Figure 8. Photoluminesce (PL) spectra of ZnO nanowires for samples #1–5 with provoking line at 325 nm.

improving of solar cell efficiency. The results emphasize that the elevation of efficiency corresponding to the most intense peak at (100).

Figure 7 displays the optical absorption spectra of the ZnO nanowire solutions (in the ethanol) characterizing by UV–visible spectrophotometer. In fact, the ZnO nanowires mostly absorb the emission over the ultraviolet and visible spectral range from 280 to 550 nm. The samples #1 and #2 (with the smallest diameter and preferring growth direction of 100) demonstrate the smallest absorbance. Figure 8 plots the PL spectra of ZnO nanowires using the excitation wavelength at 325 nm for all samples of interest. This delineates a couple of major distinct luminescence emissions namely, a narrow UV–blue band and a broad green–yellow band (deep-level emission) [21–23]. The near-band-edge (NBE) emission lies at UV range, whose peak is mainly dependent on the crystalline degree [24]. The other peak is relatively broad over the visible region due to the vacancies [21, 22]. It is supposed to identify the singly ionized oxygen and Zn vacancies which arise from the recombination nature of the photo generated holes and electrons in the defects [21, 22]. The oxygen vacancies in ZnO are actually doubly ionized species that is most likely responsible for the desirable *n*-type conductivity [23, 25, 26]. Many researchers explain that the peaks around 510 and 535 nm are related to the oxygen vacancies [21–23]. In fact, it is the recombination of a delocalized electron close to the conduction band with a deeply trapped hole in the singly ionized oxygen vacancy [21–28]. Vanheusden *et al* [29] observed a good correlation between the green emission intensity, the free-carrier concentration, and the density of oxygen vacancy in the bulk ZnO. Indeed, the green luminescence resembles to be a consequence of the electronic transition from the

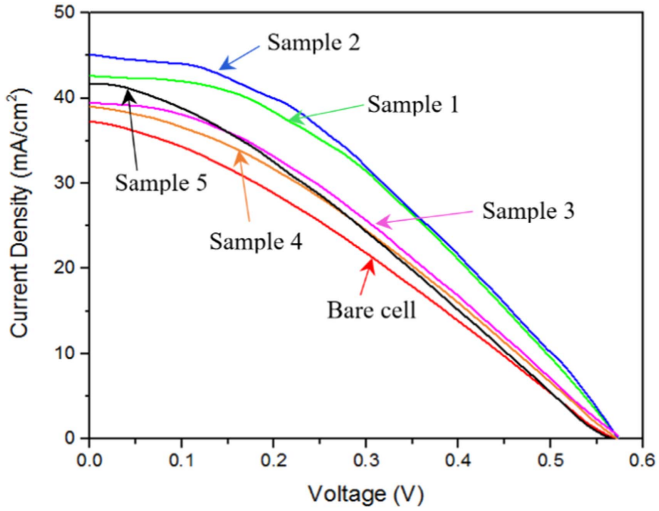

Figure 9. Current–voltage (I–V) characteristics of the untreated and treated solar cells for samples #1–5 under solar radiation (100 mW cm^{-2}).

Table 4. Electrical properties of the of ZnO nano-wire assisted Si-solar cell.

	V_{oc} (V)	J_{sc} (mA cm^{-2})	FF	Eff (%)
Reference (untreated)	0.57	37	32	6.8
Sample #1	0.57	43	40	9.8
Sample #2	0.57	45	38	9.7
Sample #3	0.57	40	35	8
Sample #4	0.57	39	34	7.5
Sample #5	0.57	42	32	7.7

NBE and exciton states to zinc and oxygen vacancies. Regarding the data, a spectral red shift lucidly takes place due to the vacancies in ZnO. The corresponding XRD attest, there is good agreement between the size of ZnO nano-wires (using the Williamson–Hall equation [18]) as well as spacing of crystalline planes according to samples #2 and #3 and the intensity of green–yellow band in PL spectroscopy. This may be due to the enhanced surface defects in terms of the surface/volume ratio [20].

Furthermore, the QY of samples #1 and #3 are measured. The fluorescence QY is an intrinsic property of a fluorophore to be important for the characterization of the novel fluorescent probes. The fluorescence QY is the ratio of the number of photons absorbed to those photons emitted through the fluorescence events. The QY of the unknown sample is determined by making use of the single point method [30, 31]:

$$Q = Q_R \frac{I}{I_R} \frac{OD_R}{OD} \frac{n^2}{n_R^2}, \tag{3}$$

where Q, I, n and OD are fluorescence QY, the integrated fluorescence intensity, the refractive index of solvent, and the optical density (absorption), respectively. The subscript R refers to the reference fluorophore of the known QY. The Ethanol is used for both reference and unknown samples as a solvent and, (n_2/n_{2R}) will be unity. Rhodamine 6G is dissolved in ethanol (QY = 95%) as. The absorbance values at the excitation wavelength of the solution are recorded by UV–Vis spectrophotometer. PL emission spectra of the solution are measured by the spectro fluorometer under excitation wavelength at 325 nm. The integrated PL intensity is the area under the PL graph over the spectral range of 350–600 nm. The calculated values for samples #1 and #3 are given to be 60% and 70% respectively.

Figure 9 depicts the I–V plots of the solar cells before (and after) dropping of ZnO nano-wires. The parameters such as the short circuit current density (J_{sc}), open circuit voltage (V_{oc}), FF, and efficiency (η) are given in table 4. The cells which are coated by the ZnO nanowires exhibit better performance with respect to the untreated one. The samples #1 and #2 demonstrate higher efficiencies as to the short-circuit current density (J_{sc}) rises from 37 to 43 and 45 mA cm^{-2}, respectively. The FF increases from 32% to 40% (and 38%) for sample #1 (and 2). Thus the efficiency scales up from 6.8% to ~9.8% for both of them. Figure 10 represents the I–V photovoltaic (PV) characteristics of a typical sample #1 against the untreated one. V_{oc} implies the function of

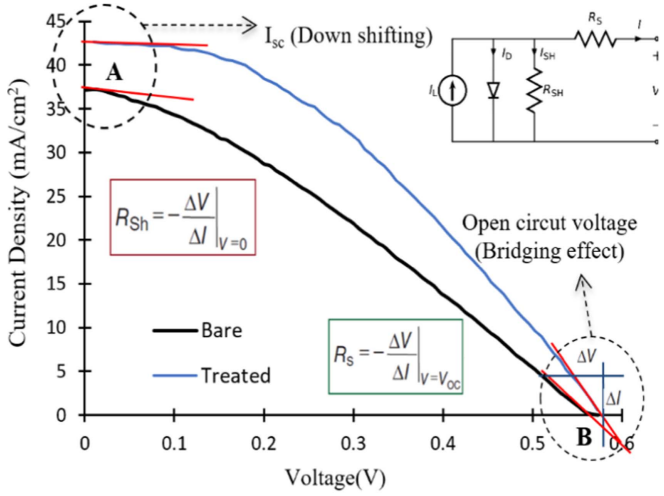

Figure 10. Typical *I–V* characteristics: equivalent series resistance (R_S) and shunt resistance (R_{sh}) for the untreated and treated solar cell (sample #1) obtained from *I–V* characteristics.

bandgap. The nanostructures generate excessive carriers and efficiently collect charges. As a consequence, the ZnO nanostructures negligibly influence the bandgap and also equivalent shunt resistance of the p–n junction. In fact, the drop coating method is a surface treatment; therefore this process does slightly change the p–n junction. Altogether, V_{oc}'s remain invariant.

The rise of I_{sc} most likely gives rise to the large absorbance of the solar radiation that mainly is due to the drop casting of ZnO nanowires on the solar cell surface. The shape of the *I–V* graph is sensitive to either the equivalent series resistance (R_s) or the shunt resistance (R_{sh}). The series resistance R_s is written as below [32]:

$$R_s = \lim_{V_{out}\to\infty}\left\{\frac{dV_{out}}{dI_{out}}\right\}. \tag{4}$$

At higher bias voltages, the series resistance R_s becomes dominant, where the space charge is neglected. At small R_s, a high current flows through the cell (even at low applied voltage); whereas the large shunt resistance R_{sh} undergoes a photocurrent leakage. The series resistance R_s includes the ohmic loss in the front contacts, the metal-semiconductor interface as well as the bulk equivalent resistance of the PV device. Conversely, the leak current at the edge of the solar cell as well as any short circuit across the p–n junction are together modeled as the shunt resistance (R_{Sh}). To obtain a large FF for an efficient power conversion, a very low series resistance (ideally zero) and a large shunt resistance (approaching to infinity) are desirable. When the nano-scale semi-conductive is dispersed over the Si surface, the equivalent series resistance R_s is drastically reduced based on the *I–V* characteristics. This flattens the curve and enlarges the FF (and efficiency) [33]. The nanowires induce to generate both excessive carriers and efficiently collect the charge. As a consequence, the ZnO nanowires negligibly influences on the shunt resistance of the p–n junction, while those with small diameters strongly cause to reduce the series resistance in the same time.

In general, according to the *I–V* characteristics, intensity of green–yellow band at PL spectroscopy as well as smaller absorbance and the corresponding to smaller of ZnO nano-wires (regarding SEM images) are affected to increase I_{sc} intensity and to decrease R_s respectively. According to PL results, the down-shifting of the solar emissions from UV to green wavelength arises from provoking various lines. The frequency conversion to the longer wavelengths, especially the green light, certainly improves the performance of solar cells. ZnO nanowires coating on the Si-solar cell partly induces the down-shifting effect to enhance the generation of the electron–hole pairs beneath deeper layer within p–n junction and mostly contributes to trap more photons leading to raise the quantum efficiency. Here, downshifting exhibits a negligible impact on the performance, as expected. Conversely, The nanowires enhances the photon trapping rather than absorbance leading to more effective events of electron–hole generation in p–n junctions that lead to elevate the efficiency [27].

Moreover, this is in good agreement with DRS spectra as shown in figure 11, where the high absorbance appears over 350–450 nm. For all samples I_{sc} could be significantly improved according to the simultaneous ZnO nanowires down-shifting, the spectral reflectance reduction and photon trapping nature.

Moreover, the EQE is applied to assess the solar cell performance in red/green/blue wavelengths i.e., at the $400 \pm 15, 460 \pm 15, 505 \pm 15, 530 \pm 15$ and 630 ± 15 nm. Table 5 tabulates the data taken from EQE analyses at certain wavelengths. It represents a discrepancy of EQE for the blue regions before (and after) ZnO

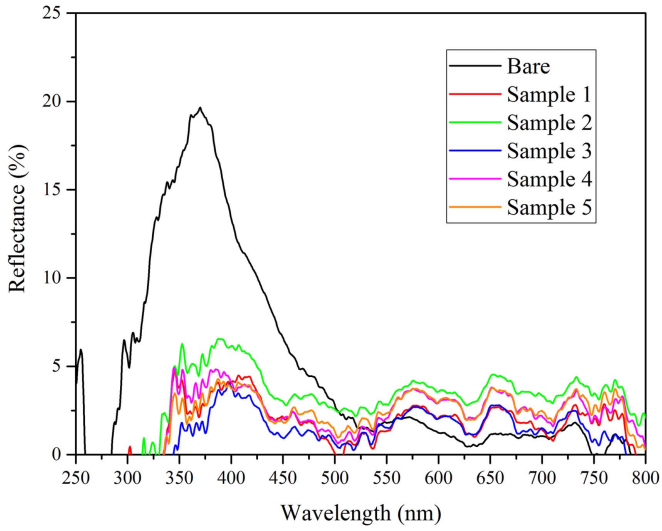

Figure 11. Spectral reflectance (DRS) of the untreated and treated solar cells.

Table 5. EQE for several tuned lights before and after exposure at 400 ± 15, 460 ± 15, 505 ± 15, 530 ± 15 and 630 ± 15 nm.

EQE	630 ± 10 nm	530 ± 10 nm	505 ± 10 nm	420 ± 10 nm	400 ± 10 nm
Bare	60	64	62	51	50
Sample #1	61	64	67	59	58
Sample #2	65	67	68	60	59
Sample #3	60	64	62	61	61
Sample #4	60	64	63	60	55
Sample #5	60	64	63	57	54

Table 6. IQE calculated from EQE and DRS analysis.

IQE	630 ± 10 nm	530 ± 10 nm	505 ± 10 nm	420 ± 10 nm	400 ± 10 nm
Bare	62	65	63	57	57
Sample #1	62	66	67	60	60
Sample #2	67	69	70	61	64
Sample #3	61	65	63	60	57
Sample #4	60	65	63	60	57
Sample #5	60	64	62	59	57

nanowire drop-casting. The PL spectra attest the increase in EQE at the blue region against the longer wavelengths. The IQE is measured using DRS and EQE results given by [34, 35]:

$$\mathrm{IQE} = \frac{\mathrm{EQE}}{1 - R} = \frac{\mathrm{EQE}}{A}. \tag{5}$$

Table 6 tabulates the calculated values as well.

Totally, there are three sensitive factors, i.e. R_s and down-shifting and photon trapping to obtain larger FF and higher efficiency.

Conclusions

ZnO nanowires are grown by TCVD method and their properties are assessed for better solar cell performance. The oxygen flow rate strongly affects the structural and optical properties of ZnO nanowires. The reduction of oxygen flow rate leads to decrease the mean nanowire diameter in the samples according to SEM micrographs. XRD patterns indicate that the highest peak appears on (100) and (101) according to smallest diameters and the larger diameters, respectively. In addition XRD demonstrates that the sample #3 exhibits the shortest spacing of

crystalline planes as well as the largest strains. Moreover, the PL spectra lucidly attest the frequency shift to the longer wavelengths. In fact, the oxygen vacancies convert the short wavelength of solar radiation to the green part of emission, leading to the larger free-carrier population for the purpose of the efficient performance. Samples #2 and #3 with largest green emissions are in good agreements with XRD data including the shortest spacing and largest strain. Furthermore, *I–V* characteristic plots larger FF due to R_s drop and higher efficiency when the solar cell is covered by ZnO nanowires with smaller diameter. Despite the reduction of the reflectance is a key parameter; however the down-shifting, absorbance over 350–520 nm, taken by UV–Vis analysis as well as R_s dropping, scale up the efficiency. This mainly arises from the skin recombination nature of the electron–hole pairs over the UV–blue region (down shifting as well as smaller absorbance over visible light) and also bridging effect of nanowires at small diameters (R_s decrease). In addition, EQE and IQE also leads to convert the short wavelength of solar radiations into the longer wavelengths and photon trapping in ZnO nanowires related to the larger generation rates of carriers. Despite we introduce these competitive phenomena involved for better performance of Si-Solar cells, however our previous works emphasizes the drop casting of nanoplates on Si solar cells leading to the efficiency enhancement due to dominant down shifting. Here, we focus on nanowire drop casting on Si solar cells that gives rise to the lucid efficiency elevation which arises from the photons trapping nature of nanowires at various spectral absorbance for making use of these findings.

Acknowledgments

The authors gratefully acknowledge the financial support of the Iran Science Elites Federation under grant 11/66332 dated 2015/05/20, and the Research Council of Imam Khomeini International University.

ORCID iDs

A Gholizadeh https://orcid.org/0000-0002-7046-114X
S Z Mortazavi https://orcid.org/0000-0002-4420-6655

References

[1] Özgür Ü, Alivov Y I, Liu C, Teke A, Reshchikov M, Doğan S, Avrutin V, Cho S-J and Morkoc H 2005 A comprehensive review of ZnO materials and devices *J. Appl. Phys.* **98** 041301
[2] Pietruszka R, Witkowski B, Gieraltowska S, Caban P, Wachnicki L, Zielony E, Gwozdz K, Bieganski P, Placzek-Popko E and Godlewski M 2015 New efficient solar cell structures based on zinc oxide nanorods *Sol. Energy Mater. Sol. Cells* **143** 99–104
[3] Feng Z, Jia R, Dou B, Li H, Jin Z, Liu X, Li F, Zhang W and Wu C 2015 Enhanced properties of silicon nano-textured solar cells enabled by controlled ZnO nanorods coating *Sol. Energy* **115** 770–6
[4] Gholizadeh A, Reyhani A, Parvin P and Mortazavi S 2017 Efficiency enhancement of ZnO nanostructure assisted Si solar cell based on fill factor enlargement and UV–blue spectral down-shifting *J. Phys. D: Appl. Phys.* **50** 185501
[5] Yu X, Yu X, Zhang J, Zhang D, Chen L and Long Y 2017 Light-trapping Al-doped ZnO thin films for organic solar cells *Sol. Energy* **153** 96–103
[6] Patel M, Kim H-S, Kim J, Yun J-H, Kim S J, Choi E H and Park H-H 2017 Excitonic metal oxide heterojunction (NiO/ZnO) solar cells for all-transparent module integration *Sol. Energy Mater. Sol. Cells* **170** 246–53
[7] Raja M, Muthukumarasamy N, Velauthapillai D, Balasundaraprabhu R, Agilan S and Senthil T S 2014 Studies on bundle like ZnO nanorods for solar cell applications *Sol. Energy* **106** 129–35
[8] Luong C H, Kim S, Surabhi S, Vo T S, Lee K-M, Yoon S-G, Jeong J-H, Choi J-H and Jeong J-R 2015 Fabrication of undoped ZnO thin film via photosensitive sol–gel method and its applications for an electron transport layer of organic solar cells *Appl. Surf. Sci.* **351** 487–91
[9] Periyat P and Ullattil S 2015 Sol–gel derived nanocrystalline ZnO photoanode film for dye sensitized solar cells *Mater. Sci. Semicond. Process.* **31** 139–46
[10] Nowak R-E, Vehse M, Sergeev O, von Maydell K and Agert C 2014 ZnO nanorod arrays as light trapping structures in amorphous silicon thin-film solar cells *Sol. Energy Mater. Sol. Cells* **125** 305–9
[11] Di Mauro A, Fragalà M E, Privitera V and Impellizzeri G 2017 ZnO for application in photocatalysis: from thin films to nanostructures *Mater. Sci. Semicond. Process.* **69** 44–51
[12] Muchuweni E, Sathiaraj T S and Nyakotyo H 2017 Low temperature synthesis of ZnO nanowires on GAZO thin films annealed at different temperatures for solar cell application *Mater. Sci. Semicond. Process.* **68** 80–6
[13] Fan R-H, Zhu L-H, Peng R-W, Huang X-R, Qi D-X, Ren X-P, Hu Q and Wang M 2013 Broadband antireflection and light-trapping enhancement of plasmonic solar cells *Phys. Rev.* B **87** 195444
[14] Lee Y-J, Ruby D S, Peters D W, McKenzie B B and Hsu J W 2008 ZnO nanostructures as efficient antireflection layers in solar cells *Nano Lett.* **8** 1501–5
[15] Hussain B, Ebong A and Ferguson I 2015 Zinc oxide as an active n-layer and antireflection coating for silicon based heterojunction solar cell *Sol. Energy Mater. Sol. Cells* **139** 95–100
[16] Parvin P, Reyhani A, Mehrabi M, Refahizadeh M, Mortazavi S and Ranjbar A 2017 Efficiency enhancement using ArF laser induced micro/nanostructures on the polymeric layer of solar cell *Opt. Laser Technol.* **88** 242–9
[17] Zhang X, Qin J, Xue Y, Yu P, Zhang B, Wang L and Liu R 2014 Effect of aspect ratio and surface defects on the photocatalytic activity of ZnO nanorods *Sci. Rep.* **4** 4596

[18] Prabhu Y T, Rao K V, Kumar V S S and Kumari B S 2013 Synthesis of ZnO nanoparticles by a novel surfactant assisted amine combustion method *Adv. Nanopart.* **2** 45
[19] Jun M-C, Park S-U and Koh J-H 2012 Comparative studies of Al-doped ZnO and Ga-doped ZnO transparent conducting oxide thin films *Nanoscale Res. Lett.* **7** 639
[20] Kunj S, Sreenivas K, Chitra R, Bhattacharya S and Sahoo N 2016 Defect free *C*-axis oriented zinc oxide (ZnO) films grown at room temperature using RF magnetron sputtering *AIP Conf. Proc.* 1731, 080048
[21] Jin B, Bae S, Lee S and Im S 2000 Effects of native defects on optical and electrical properties of ZnO prepared by pulsed laser deposition *Mater. Sci. Eng.* B **71** 301–5
[22] Lin B, Fu Z and Jia Y 2001 Green luminescent center in undoped zinc oxide films deposited on silicon substrates *Appl. Phys. Lett.* **79** 943–5
[23] Liu L, Mei Z, Tang A, Azarov A, Kuznetsov A, Xue Q-K and Du X 2016 Oxygen vacancies: the origin of n-type conductivity in ZnO *Phys. Rev.* B **93** 235305
[24] Bagnall D, Chen Y, Zhu Z, Yao T, Shen M and Goto T 1998 High temperature excitonic stimulated emission from ZnO epitaxial layers *Appl. Phys. Lett.* **73** 1038–40
[25] Zeng Z, Petoni A, Garoufalis C S, Baskoutas S and Bester G 2015 Near-band-edge exciton polarization change in ZnO nanowires *Phys. Chem. Chem. Phys.* **17** 1197–203
[26] Rajalakshmi M, Sohila S, Ramya S, Divakar R, Ghosh C and Kalavathi S 2012 Blue green and UV emitting ZnO nanoparticles synthesized through a non-aqueous route *Opt. Mater.* **34** 1241–5
[27] Bagnall D, Chen Y, Shen M, Zhu Z, Goto T and Yao T 1998 Room temperature excitonic stimulated emission from zinc oxide epilayers grown by plasma-assisted MBE *J. Cryst. Growth* **184** 605–9
[28] Umar A, Suh E-K and Hahn Y 2006 Non-catalytic growth of high aspect-ratio ZnO nanowires by thermal evaporation *Solid State Commun.* **139** 447–51
[29] Vanheusden K, Warren W, Seager C, Tallant D, Voigt J and Gnade B 1996 Mechanisms behind green photoluminescence in ZnO phosphor powders *J. Appl. Phys.* **79** 7983–90
[30] Joseph R L and Lakowicz R 1999 *Principles of Fluorescence Spectroscopy* (New York: Kluwer Academic/Plenum Publishers)
[31] Yang W, Yang H, Ding W, Zhang B, Zhang L, Wang L, Yu M and Zhang Q 2016 High quantum yield ZnO quantum dots synthesizing via an ultrasonication microreactor method *Ultrason. Sonochem.* **33** 106–17
[32] Huynh W U, Dittmer J J, Teclemariam N, Milliron D J, Alivisatos A P and Barnham K W 2003 Charge transport in hybrid nanorod-polymer composite photovoltaic cells *Phys. Rev.* B **67** 115326
[33] Mertens K 2013 *Photovoltaics: Fundamentals, Technology and Practice* (New York: Wiley)
[34] Kirchartz T, Ding K and Rau U 2016 Fundamental electrical characterization of thin-film solar cells *Advanced Characterization Techniques for Thin Film Solar Cells* vol 1 (Weinheim: Wiley) ch 2 41–69
[35] Poortmans J and Arkhipov V 2006 *Thin Film Solar Cells: Fabrication, Characterization and Applications* vol 5 (New York: Wiley)